

# Partition Decoupling for Multi-gene Analysis of Gene Expression Profiling Data

Rosemary Braun<sup>1</sup>, Gregory Leibon<sup>2</sup>, Scott Pauls<sup>2</sup>, and Daniel Rockmore<sup>2,3</sup>

<sup>1</sup> *National Cancer Institute, NIH, Bethesda, MD 20892*

<sup>2</sup> *Department of Mathematics, Dartmouth College, Hanover, NH 03755*

<sup>3</sup> *The Santa Fe Institute, Santa Fe, NM 87501*

October 30, 2021

## Abstract

We describe an extension and application of a new unsupervised statistical learning technique, known as the Partition Decoupling Method (PDM), to gene expression microarray data. This method may be used to classify samples based on multi-gene expression patterns and to identify pathways associated with phenotype, without relying upon the differential expression of individual genes.

The PDM uses iterated spectral clustering and scrubbing steps, revealing at each iteration progressively finer structure in the geometry of the data. Because spectral clustering has the ability to discern clusters that are not linearly separable, its performance is superior to distance- and tree-based classifiers. After projecting the data onto the cluster centroids and computing the residuals (“scrubbing”), one can repeat the spectral clustering, revealing clusters that were not discernible in the first layer. These iterations, each of which provide a partition of the data that is decoupled from the others, are carried forward until the structure in the residuals is indistinguishable from noise, preventing over-fitting.

This technique is particularly suitable in the context of gene expression data from complex diseases, where phenotypes are not linearly separable and multi-gene effects are likely to play a role. Because spectral clustering employs a low-dimension embedding of the data, the combined effect of a large number of genes may be simultaneously considered. Both the dimensionality of the embedding and the number of clusters are determined from the data, yielding an entirely unsupervised classification method. Here, we describe the PDM in detail and apply it to three publicly available cancer gene expression data sets. Our results demonstrate that the PDM is able to distinguish cell types and treatments with higher accuracy than is obtained through other approaches. By applying the PDM on a pathway-by-pathway basis and searching for pathways that permit unsupervised clustering that accurately matches known sample characteristics, we show how the PDM may be used to find sets of mechanistically-related genes that may play a role in disease.

## Introduction

Since their first use nearly fifteen years ago [1], microarray gene expression profiling experiments have become a ubiquitous tool in the study of disease. The vast number of gene transcripts assayed by modern microarrays ( $10^5$ – $10^6$ ) has driven forward our understanding of biological processes tremendously, both by elucidating mechanisms at play in specific phenotypes and by revealing previously unknown regulatory mechanisms at

play in all cells. However, the high-dimensional data produced in these experiments—often comprising many more variables than samples and subject to noise—presents analytical challenges.

The analysis of gene expression data can be broadly grouped into two categories: the identification of differentially expressed genes (or gene-sets) between two or more known conditions, and the unsupervised identification (clustering) of samples or genes that exhibit similar profiles across the data set. In the former case, each gene is tested individually for association with the phenotype of interest, adjusting at the end for the vast number of genes probed. Pre-identified gene sets, such as those fulfilling a common biological function, may then be tested for an overabundance of differentially expressed genes (e.g., using gene set enrichment analysis [2]); this approach aids biological interpretability and improves the reproducibility of findings between microarray studies. In clustering, the hypothesis that functionally related genes and/or phenotypically similar samples will display correlated gene expression patterns motivates the search for groups of genes or samples with similar expression patterns. The most commonly used algorithms are hierarchical clustering [3],  $k$ -means clustering [4, 5] and Self Organizing Maps [6]. A brief overview may be found in [7]. Of these,  $k$ -means appears to perform the best [7, 8, 9]. Relatedly, gene shaving [10] searches for clusters of genes showing both high variation across the samples and correlation across the genes, and several biclustering algorithms (such as [11]) search for class-conditional clusters of correlated genes. These methods are simple, visually appealing, and have identified a number of co-regulated genes and phenotype classes.

While approaches have been fruitful, they also have the potential to miss causative mechanisms that can be affected by a change in any one of several genes (such that no single alteration reaches significance) as well as mechanisms that require the concerted activity of multiple genes to produce a specific phenotype. It is well known that complex diseases, such as cancers, exhibit considerable molecular heterogeneity for the above reasons [12]. As a result, individual genes may fail to reach significance, and lists of differentially expressed genes or gene signatures may have poor concordance across studies. Additionally, pathway analyses that rely on single-gene association statistics (such as GSEA [2]) may fail to identify causative mechanisms. For the same reasons, clustering algorithms that rely on linearly-separable clusters (and hence upon differential expression between the clusters) may fail to partition the samples in a manner that reflects the true underlying biology.

As an example of how causative genes can be missed in gene-centric analyses, consider a recent study in which gene expression profiles in the Wagyu cattle are compared to those of the double-musclcd Piedmontese cattle [13]. The Piedmontese cattle’s muscular hypertrophy is attributable to a nonfunctional mutation of the myostatin gene (MSTN), but because MSTN itself is not differentially expressed between the two bovine models, its biological role cannot be inferred using traditional analyses of gene expression data. On the other hand, [13] showed that the functional MSTN variant was *co*-expressed with its regulatory target MYL2 in Wagyu cattle, whereas the nonfunctional variant in the Piedmontese cattle did not exhibit co-expression with MYL2. The correct identification of this system, in absence of differential expression at the gene level in MSTN or MYL2, is crucial to understanding the molecular determinants of the double-musclcd phenotype. This example serves to underscore the pressing need for analysis methods that can reveal *systems-level* differences in cases and controls even when the constituent genes do not exhibit differential expression.

As an alternative approach, we propose here an analysis technique that is designed to reveal relationships between samples based on multi-gene expression profiles without requiring that the genes be differentially

expressed (i.e., without requiring the samples to be linearly separable in the gene-expression space), and that has the power to reveal relationships between samples at various scales, permitting the identification of phenotypic subtypes. Our approach adapts a new unsupervised machine-learning technique, the Partition Decoupling Method (PDM) [14, 15], to gene expression data. The PDM consists of two iterated components: a spectral clustering step, in which the correlations between samples in the high-dimensional feature space is used to partition samples into clusters, followed by a scrubbing step, in which a projection of the data onto the cluster centroids is removed so that the residuals may be clustered. As part of the spectral clustering procedure, a low-dimensional nonlinear embedding of the data is used; as we will show in the Methods section, this both reduces the effect of noisy features and permits the partitioning of clusters with non-convex boundaries. The clustering and scrubbing steps are iterated until the residuals are indistinguishable from noise, as determined by comparison to a resampled null model. This procedure yields “layers” of clusters that articulate relationships between samples at progressively finer scales, and distinguishes the PDM from other clustering algorithms.

The PDM has a number of satisfying features. The use of spectral clustering allows identification of clusters that are not necessarily separable by linear surfaces, permitting the identification of complex relationships between samples. This means that clusters of samples can be identified even in situations where the genes do not exhibit differential expression, a trait that makes it particularly well-suited to examining gene expression profiles of complex diseases. The PDM employs a low-dimensional embedding of the feature space, reducing the effect of noise in microarray studies. Because the data itself is used to determine both the optimal number of clusters and the optimal dimensionality in which the feature space is represented, the PDM provides an entirely unsupervised method for classification without relying upon heuristics. Importantly, the use of a resampled null model to determine the optimal dimensionality and number of clusters prevents clustering when the geometric structure of the data is indistinguishable from chance. By scrubbing the data and repeating the clustering on the residuals, the PDM permits the resolution of relationships between samples at various scales; this is a particularly useful feature in the context of gene-expression analysis, as it permits the discovery of distinct sample subtypes. By applying the PDM to gene subsets defined by common pathways, we can use the PDM to identify gene subsets in which biologically-meaningful topological structures exist, and infer that those pathways are related to the clinical characteristics of the samples (for instance, if the genes in a particular pathway admit unsupervised PDM partitioning that corresponds to tumor/non-tumor cell types, one may infer that pathway’s involvement in tumorigenesis). This pathway-based approach has the benefit of incorporating existing knowledge and being interpretable from a biological standpoint in a way that searching for sets of highly significant but mechanistically unrelated genes does not.

A number of other operationally similar, yet functionally distinct, methods have been considered in the literature. First, simple spectral clustering has been applied to gene expression data in [9], with mixed success. The PDM improves upon this both through the use of the resampled null model to provide a data-driven (rather than heuristic) choice of the clustering parameters, and by its ability to articulate independent partitions of the data (in contrast to a single layer) where such structure is present. As we will show, these aspects make PDM more powerful than standard spectral clustering, yielding improved accuracy as well as the potential to identify sample subtypes that are not already known. Another novel clustering method is proposed in [16], where an adaptive distance norm is used that can be shown to identify clusters of different

shapes. The algorithm iteratively assigns clusters and refines the distance metric scaling parameter in a cluster-conditional fashion based on each cluster’s geometry. This approach is able to identify clusters of mixed sizes and shapes that cannot be discriminated using fixed Euclidean or Mahalanobis distance metrics, and thus is a considerable improvement over  $k$ -means clustering. However, the method as described in [16] is computationally expensive and cannot identify non-convex clusters as spectral clustering, and hence the PDM, can. Alternatively, SPACC [17] uses the same type of non-linear embedding of the data as is used in the PDM, which permits the articulation of non-convex boundaries. In SPACC [17], a single dimension of this embedding is used to recursively partition the data into two clusters. The partitioning is carried out until each cluster is solely comprised of one class of samples, yielding a classification tree. In this way, SPACC may also in some cases permit partitioning of known sample classes into subcategories. However, SPACC differs from the PDM in two crucial ways. First, the PDM’s use of a data-determined number of informative dimensions permits more accurate clusterings than those obtained from a single dimension in SPACC. Second, SPACC is a semi-supervised algorithm that uses the known class labels to set a stopping threshold. Because there is no comparison to a null model, as in the PDM, SPACC will partition the data until the clusters are pure with respect to the class labels. This means that groups of samples with distinct molecular subtypes but identical class labels will remain unpartitioned (SPACC cannot be used to reveal novel subclasses) and that groups of samples with differing class labels but indistinguishable molecular characteristics will be artificially divided until the purity threshold is reached. In this respect, the PDM improves on SPACC by “letting the data speak.” A fourth approach, QUBIC [11] is a graph theoretic algorithm that identifies sets of genes with similar class-conditional coexpression patterns (biclusters) by employing a network representation of the gene expression data and agglomeratively finding heavy subgraphs of co-expressed genes. In contrast to the unsupervised clustering of the PDM, QUBIC is a supervised method that is designed to find gene subsets with coexpression patterns that differ between pre-defined sample classes. In [11] it is shown that QUBIC is able to identify functionally related gene subsets with greater accuracy than competing biclustering methods; still, QUBIC is only able to identify biclusters in which the genes show strict correlation or anticorrelation coexpression patterns, which means that gene sets with more complex coexpression dynamics cannot be identified. The PDM is thus unique in a number of ways: not only is it able to partition clusters with nonlinear and nonconvex boundaries, it does so in an unsupervised manner (permitting the identification of unknown subtypes) and in the context of comparison to a null distribution that both prevents clustering by chance and reduces the influence of noisy features. Moreover, the PDM’s iterated clustering and scrubbing steps permit the identification of independent (i.e., decoupled) partitions in the data.

In this manuscript, we describe the PDM algorithm and demonstrate its application to several publicly-available gene-expression data sets. To illustrate the PDM’s ability to articulate independent partitions of samples, we apply it to genome-wide expression data from a four phenotype, three exposure radiation response study [18]. The PDM partitions the samples by exposure and then by phenotype, yielding higher accuracy for predictions of radiation sensitivity than previously reported [18]. We also compare the PDM results to those obtained in a recent [9] comparison of clustering techniques, demonstrating the PDM’s ability to identify cancer subtypes from global patterns in the gene expression data. Next, we apply the PDM using gene subsets defined by pathways rather than the global gene expression data, demonstrating how the PDM can be used to find biological mechanisms that relate to the phenotype of interest. We demonstrate pathway-PDM in both the radiation response data [18] as well as a larger prostate cancer data

set [19]. Our results suggest that the PDM is a powerful tool for articulating relationships between samples and for identifying pathways containing multi-gene expression patterns that distinguish phenotypes.

## Methods

### Partition Decoupling Algorithm

The partition decoupling method (PDM) was first described in [14]. We summarize it here, and discuss its application to gene-expression data. The PDM consists of two iterated submethods: the first, spectral clustering, finds the dominant structures within the system, while the second “scrubbing” step removes this structure such that the next clustering iteration can distinguish finer-scale relationships within the residual data. The two steps are repeated until the residuals are indistinguishable from noise. By performing successive clustering steps, factors contributing to the partitioning of the data at different scales may be revealed.

### Spectral Clustering

The first step, spectral clustering, serves to identify clusters of samples in high-dimensional gene-expression space. The motivation is simple: given a set of samples and a measure of pairwise similarity  $s_{i,j}$  between each pair, we wish to partition the data such that samples within one cluster are similar to each other based on their gene expression profiles. A summary of the spectral clustering algorithm is given in Table 1.

Spectral clustering offers several advantages over traditional clustering algorithms such as those reviewed in [7]. Most importantly, no constraint is placed on the geometry of the data, in contrast to the tree-like structure imposed by hierarchical clustering [3] or the requirement that clusters be convex in the feature space when using distance-based  $k$ -means clustering [4, 5] and Self Organizing Maps [6]. Spectral clustering also uses a low-dimensional embedding of the data, thus excluding the noisy, high-frequency components.

In spectral clustering, the data are represented as a complete graph in which nodes correspond to samples and edge weights  $s_{i,j}$  correspond to some measure of similarity between a pair of nodes  $i$  and  $j$ . Spectral graph theory (see, e.g., [20]) is brought to bear to find groups of connected, high-weight edges that define clusters of samples. This problem may be reformulated as a form of the min-cut problem: cutting the graph across edges with low weights, so as to generate several subgraphs for which the similarity between nodes is high and the cluster sizes preserve some form of balance in the network. It has been demonstrated [20, 21, 22] that solutions to relaxations of these kinds of combinatorial problems (i.e., converting the problem of finding a minimal configuration over a very large collection of discrete samples to achieving an approximation via the solution to a related continuous problem) can be framed as an eigendecomposition of a graph Laplacian matrix  $\mathbf{L}$ . In particular, we use the Laplacian matrix formed from the adjacency matrix  $\mathbf{S}$  (comprised of  $s_{i,j}$ ) and the diagonal degree matrix  $\mathbf{D}$  with elements  $d_i = \sum_j s_{i,j}$ :

$$\mathbf{L} = \mathbf{I} - \mathbf{D}^{-1/2} \mathbf{S} \mathbf{D}^{-1/2} . \tag{1}$$

The similarity measure between two data points is computed (as in [15]) from their correlation  $\rho_{i,j}$  by first

converting the correlation to a chord distance on the unit sphere and then exponentiating,

$$s_{i,j} = \exp \left( \frac{-\left( \sin \left( \arccos(\rho_{i,j})/2 \right) \right)^2}{\sigma^2} \right), \quad (2)$$

where  $\sigma$  determines how quickly  $s_{i,j}$  falls off with the correlation  $\rho_{i,j}$  and may be tuned to reveal structure at various scales of the system.

The spectrum of  $\mathbf{L}$  contains information regarding the graph connectivity. Specifically, the number of zero-value eigenvalues corresponds to the number of connected components; since we have a complete graph, there will be exactly one. The second-smallest eigenvalue and its associated eigenvector (the so-called Fiedler value  $\lambda_1$  and vector  $v_1$ ) encodes a coarse geometry of the data, effectively the coordinates for the “best” (in the sense of clustering) one-dimensional embedding of the network. Successive eigenvectors enable the articulation of finer resolution. By embedding the data into a smaller-dimensional space defined by the low-frequency eigenvectors and clustering the embedded data, the geometry of the data may be revealed.

The embedded data are then be clustered using  $k$ -means [4]. Because  $k$ -means clustering is by nature stochastic [4], multiple  $k$ -means runs are performed and the clustering yielding the smallest within-cluster sum of squares is chosen. In order to use  $k$ -means on the embedded data, two parameters need to be chosen: the number of eigenvectors  $l$  to use (that is, the dimensionality of the embedded data) and the number of clusters  $k$  into which the data will be clustered.

**Optimization of  $l$**  The optimal dimensionality of the embedded data is obtained by comparing the eigenvalues of the Laplacian to the distribution of Fiedler values expected from null data. The motivation of this approach follows from the observation that the size of eigenvalues corresponds to the degree of structure (see [22]), with smaller eigenvalues corresponding to greater structure. Specifically, we wish to construct a distribution of null Fiedler values—eigenvalues encoding the coarsest geometry of randomly organized data—and select the eigenvalues from the true data that are significantly small with respect to this distribution (below the 0.05 quantile). In doing so, we select the eigenvalues that indicate greater structure than would be expected by chance alone. The idea is that the distribution of random Fiedler values give a sense of how much structure we could expect of a comparable random network. We thus take a collection of perpendicular axes, onto each of which the projection of the data would reveal more structure than we would expect at random.

The null distribution of Fiedler values is obtained through resampling  $s_{i,j}$  (preserving  $s_{i,j} = s_{j,i}$  and  $s_{i,i} = 1$ ). This process may be thought of as “rewiring” the network while retaining the same distribution of edge weights. This has the effect of destroying structure by dispersing clusters (subgraphs containing high edge weights) and creating new clusters by random chance. Because the raw data itself is not resampled, the resulting resampled network is one which has the same marginal gene expression distributions and gene-gene correlations as the original data, and is thus a biologically comparable network to that in the true data.

**Optimization of  $k$**  Methods for obtaining the number of clusters  $k$  suitable for partitioning a data set are an open research question (see, e.g., [22, 23] and references therein). Our approach exploits the property [15, 22] that clustering the entries in the Fiedler vector yields the best decomposition of the network components. Consequently, one can use the number peaks in the density of the Fiedler vector—that is, the

number of values about which the elements of  $v_1$  are clustered—as the number of clusters. (This procedure is roughly analogous to finding regions of high density along the first principle component of the data.) To obtain this value, we fit a Gaussian mixture model [24] with 2–30 components (assuming unequal variances), compute the Bayesian Information Criterion (BIC) for each mixture model, and choose the optimum number of components (for details of the implementation, see [25, 26]).

Once  $k$  and  $l$  have been assigned, the data embedded in the  $l$  eigenvectors is clustered using  $k$ -means [4]. The spectral clustering procedure offers several advantages over simple clustering of the original data using  $k$ -means: first, the Fiedler vector provides a natural means to estimate the number of clusters; and second, because spectral clustering operates on similarity of the samples, rather than planar cuts of the high-dimensional feature space, complex correlation structures can be identified. A complete discussion of the advantages of spectral clustering is given in [20, 21, 22].

To illustrate the power of this method, let consider a toy data set called “two\_circles” in which 200 data points are placed in two dimensional space in two concentric circles, as depicted in Fig. 1. Because  $k$ -means alone can only identify clusters with convex hulls,  $k$ -means clustering using  $k = 2$  produces an arbitrary, linear division of the data as shown in Fig. 1(a). In contrast, spectral clustering identifies the two rings as individual clusters, as seen in Fig. 1(b). While  $k$ -means took  $k = 2$  as an input from the user, the spectral clustering example determined  $k = 2$  from the data, as shown in Fig. 1(c); the rug plot depicts the distribution of the Fiedler vector coordinates, in which two peaks are readily visible and chosen as indicative of two clusters, as described above.

While the two\_circles data is simulated, we note that patterns of this type will arise when out-of-phase oscillatory genes, such as those involved in circadian rhythms or cell cycle processes, are sampled; the radii of the co-expression circles will be dictated by the amplitude of the gene oscillations. An illustration of such patterns in nature is provided in Fig. 2, which depicts the co-expression pattern of three cell-cycle related genes in CDC-28 and elutriation synchronized yeast cells from [27]. The elutriation synchronized cells exhibit much smaller amplitude oscillations than do the CDC-28 synchronized cells; while the CDC-28 and elutriation synchronized cells cannot be distinguished using  $k$ -means, the distinction is readily made via spectral clustering. The biological relevance of patterns such as those depicted in Figs. 1 and 2 has been noted in mammalian systems as well; in [28] it is found that the majority of mammalian genes oscillate and that the amplitude of oscillatory genes differs between tissue types and is associated with the gene’s function. These observations led to the conclusion in [28] that pathways should be considered as dynamic systems of genes oscillating in coordination with each other, and underscores the need to detect amplitude differences in co-oscillatory genes as depicted in Figs. 1 and 2.

The benefit of spectral clustering for pathway-based analysis in comparison to over-representation analyses such as GSEA [2] is also evident from the two\_circles example in Fig. 1. Let us consider a situation in which the  $x$ -axis represents the expression level of one gene, and the  $y$ -axis represents another; let us further assume that the inner ring is known to correspond to samples of one phenotype, and the outer ring to another. A situation of this type may arise from differential misregulation of the  $x$  and  $y$  axis genes. However, while the variance in the  $x$ -axis gene differs between the “inner” and “outer” phenotype, the means are the same (0 in this example); likewise for the  $y$ -axis gene. In the typical single-gene  $t$ -test analysis of this example data, we would conclude that neither the  $x$ -axis nor the  $y$ -axis gene was differentially expressed; if

our gene set consisted of the  $x$ -axis and  $y$ -axis gene together, it would not appear as significant in GSEA [2], which measures an abundance of single-gene associations. Yet, unsupervised spectral clustering of the data would produce categories that correlate exactly with the phenotype, and from this we would conclude that a gene set consisting of the  $x$ -axis and  $y$ -axis genes plays a role in the phenotypes of interest. We exploit this property in applying the PDM by pathway to discover gene sets that permit the accurate classification of samples.

## Scrubbing

After the clustering step has been performed and each data point assigned to a cluster, we wish to “scrub out” the portion of the data explained by those clusters and consider the remaining variation. This is done by computing first the cluster centroids (that is, the mean of all the datapoints assigned to a given cluster), and then subtracting the data’s projection onto each of the centroids from the data itself, yielding the residuals. The clustering step may then be repeated on the residual data, revealing structure that may exist at multiple levels, until either a) the eigenvalues of the Laplacian in the scrubbed data are indistinguishable from those of the resampled graph as described above; or b) the cluster centroids are linearly dependent. (It should be noted here that the residuals may still be computed in the latter case, but it is unclear how to interpret linearly dependent centroids.)

## Implementation

The PDM as described above was implemented in R [29] and applied to the following data sets. Genes with missing expression values were excluded when computing the (Pearson) correlation  $\rho_{i,j}$  between samples. In the  $l$ -optimization step, 60 resamplings of the correlation coefficients were used to determine the dimension of the embedding  $l$ . In the clustering step, 30  $k$ -means runs were performed, choosing the clustering yielding the smallest within-cluster sum of squares.

## Data

**Radiation Response Data** These data come from a gene-expression profiling study of radiation toxicity designed to identify the determinants of adverse reaction to radiation therapy [18]. In this study, skin fibroblasts from 14 patients with high radiation sensitivity (High-RS) were collected and cultured, along with those from three control groups: 13 patients with low radiation-sensitivity (Low-RS), 15 healthy individuals, and 15 individuals with skin cancer. The cells were then subject to mock (M), ultraviolet (U) and ionizing (I) radiation exposures. As reported in [18], RNA from these 171 samples comprising four phenotypes and three treatments were hybridized to Affymetrix HGU95AV2 chips, providing gene expression data for each sample for 12615 unique probes. The microarray data was normalized using RMA [30]. The gene expression data is publicly available and was retrieved from the Gene Expression Omnibus [31] repository under record number GDS968.

**DeSouto Multi-study Benchmark Data** These data comprise filtered gene expression levels from 21 cancer studies using Affymetrix microarrays along with associated class labels. The data were analyzed previously in [9], where several clustering methods were applied to compare algorithmic performance. The



data were obtained from their original sources and subjected to filtering as described in [9]; we obtained the filtered sets as used in [9] and made available by the authors. This permits a direct comparison of the PDM results to those reported in [9].

**Singh Prostate Data** These data come from a gene-expression profiling study of prostate cancer comprising 52 tumor samples (T) and 50 tumor-adjacent normal samples (N) from 52 men who had undergone radical prostatectomy [19]. RNA was hybridized to Affymetrix HGU95AV2 chips, providing gene expression data for each sample for 12615 unique probes. The microarray data CEL files were downloaded from the Broad Institute website and normalized using RMA [30].

**Pathway annotation** The BioConductor [32] annotation packages `hgu95av2.db`, `hgu95a.db`, and `KEGG.db` were used to map Affymetrix probe IDs to KEGG pathways. Only KEGG pathways were investigated. A total of 203 KEGG pathways containing genes probed in the above data were identified.

## Results

We apply the PDM to several cancer gene expression data sets to demonstrate how it may be used to reveal multiple layers of structure. In the first data set [18], the PDM articulates two independent partitions corresponding to cell type and cell exposure, respectively. The second data set [9] demonstrates how successive partitioning by the PDM can reveal disease and tissue subtypes in an unsupervised way. We then carry out Pathway-PDM to identify the biological mechanisms that drive phenotype-associated partitions. In addition to applying it to the radiation response data set mentioned above [18], we also apply Pathway-PDM to a prostate cancer data set [19], and briefly discuss how the Pathway-PDM results show improved concordance of significant pathways identified in the Singh data [19] with those previously identified in several other prostate cancer data sets [36].

### Partition Decoupling in Cancer Gene Expression Data

**Radiation Response Data** We begin by applying the PDM to the radiation response data [18] to illustrate how it may be used to reveal multiple layers of structure that, in this case, correspond to radiation exposure and sensitivity. In the first layer, spectral clustering classifies the samples into three groups that correspond precisely to the treatment type. The number of clusters was obtained using the BIC optimization method as described, and resampling the correlation coefficients was used to determine the dimension of the embedding  $l$  using 60 permutations; 30  $k$ -means runs were performed, choosing the clustering yielding the smallest within-cluster sum of squares. Classification results are given in Table 2 and Figure 3(a); the unsupervised algorithm correctly identifies that three clusters are present in the data, and assigns samples to clusters in a manner consistent with their exposure.

In order to compare the performance of spectral clustering to that of  $k$ -means, we ran  $k$ -means on the original data using  $k = 3$  and  $k = 4$ , corresponding to the number of treatment groups and number of cell type groups respectively. As with the spectral clustering, 30 random  $k$  means starts were used, and the smallest within-cluster sum of squares was chosen. The results, given in Tables 3 and 4, show substantially noisier classification than the results obtained via spectral clustering. It should also be noted that the

number of clusters  $k$  used here was not derived from the characteristics of the data, but rather assigned in a supervised way based on additional knowledge of the probable number of categories (here, dictated by the study design). While the pure  $k$ -means results are noisy, the  $k = 4$  classification yields a cluster that is dominated by the highly radiation-sensitive cells (cluster 4, Table 4). Membership in this cluster versus all others identifies highly radiation-sensitive cells with 62% sensitivity and 96% specificity; if we restrict the analysis to the clinically-relevant comparison between the last two cell types—that is, cells from cancer patients who show little to no radiation sensitivity and those from cancer patients who show high radiation sensitivity—the classification identifies radiation-sensitive cells with 62% sensitivity and 82% specificity.

The result from the  $k = 4$   $k$ -means classification suggest that there exist cell-type specific differences in gene expression between the high radiation sensitivity cells and the others. To investigate this, we perform the “scrubbing” step of the PDM, taking only the residuals of the data after projecting onto the clusters obtained in the first pass. As in the first layer, we use the BIC optimization method to determine the number of clusters  $k$  and resampling of the correlations to determine the dimension of the embedding  $l$  using 60 permutations. The second layer of structure revealed by the PDM partitioned the high-sensitivity samples from the others into two clusters. Classification results are given in Table 5 and Figure 3(b), and it can be seen that the partitioning of the radiation-sensitive samples is highly accurate (83% sensitivity; 91% specificity across all samples, 72% when comparing solely to low radiation-sensitivity patient samples).

Further PDM iterations resulted in residuals that were indistinguishable from noise (see Methods); we thus conclude that there are only two layers of structure present in the data: the first corresponding to exposure, and the second to radiation sensitivity. That is, there exist patterns in the gene expression space that distinguish UV- and ionizing radiation exposed cells from mock-treated cells (and from each other), and that there exist further patterns that distinguish high-sensitivity cells from the rest. Together, these independent (decoupled) sets of clusters describe six categories, as shown in Fig. 3(c), wherein the the second layer partitions the radiation sensitive cells from the others in each exposure-related partition. The fact that the mock-exposure as well as the UV- and IR-exposure partitions are further divided by radiation sensitivity in the second layer suggests that there exist constitutive differences in the radiation sensitive cells that distinguish them from the other groups even in the absence of exposure. Importantly, the data-driven methodology of PDM identifies only phenotypic clusters, corresponding to the high-sensitivity cells and the three control groups combined, without further subpartitioning the combined controls. This suggests that the three control groups do not exhibit significant differences in their global gene-expression profiles.

In the original analysis of this data [18], the authors used a linear, supervised algorithm (SAM, a nearest shrunken centroids classifier [33]) to develop a predictor for the high-sensitivity samples. This approach obtained 64.2% sensitivity and 100% specificity [18], yielding a clinically useful predictor. The PDM’s unsupervised detection of the high sensitivity sample cluster suggests that the accuracy in [18] was not a result of overfitting to training data; moreover, the PDM’s ability to identify those samples with higher sensitivity (83%) than in [18] indicates that there exist patterns of gene expression distinct to the radiation-sensitive patients which were not identified in the SAM analysis, but are detectable using the PDM.

**DeSouto Multi-study Benchmark Data** Having observed the PDM’s ability to decouple independent partitions in the four-phenotype, three-exposure radiation response data, we next consider the PDM’s ability to articulate disease subtypes. Because cancers can be molecularly heterogeneous, it is often important to

articulate differences between subtypes—a distinction that may be more subtle than the differences caused by radiation exposure. Here, we apply the PDM to the suite of 21 Affymetrix data sets previously considered in [9]. The use of these sets is motivated by their diversity and by the ability to compare the PDM performance to that of the methods reported in [9].

In [9], the authors applied several widely used clustering algorithms (hierarchical clustering,  $k$ -means, finite mixture of Gaussians [FMG], shared nearest-neighbor, and spectral clustering) to the data using various linkage and distance metrics as available for each. In this study, the number of clusters  $k$  was set manually ranging on  $\lceil k_c, \sqrt{n} \rceil$ , where  $k_c$  is the known number of sample classes and  $n$  is the number of samples; in the spectral clustering implementation,  $l$  was set equal to the chosen  $k$ . Note that the PDM differs from basic spectral clustering as applied in [9] several crucial ways: first,  $k$  and  $l$  are data-driven (thus permitting  $k$  that is smaller than  $k_c$ , as many dimensions  $l$  as are significant compared to the null model as previously described, and no clustering where structure is deemed non-existent compared with the null model); and second, the successive partitioning carried out in the PDM layers can disambiguate mixed clusters. Importantly, the PDM partitions are obtained without relying on prior knowledge of the number of clusters—an important feature when the data may contain un-identified disease subtypes.

To illustrate this, we focus on a handful of the benchmark data sets. (Full results are provided as supplementary information.) The partitions are shown in Fig. 4. In Fig. 4(a) and (b), PDM reveals a single layer of three clusters in two versions of the Golub-1999 leukemia data [34]. The two data sets as provided contained identical gene expression measurements and differed only in the sample status labels, with Golub-1999-v1 only distinguishing AML from ALL, but Golub-1999-v2 further distinguishing between B- and T-cell ALL. As can be seen from Fig. 4(a,b), the PDM articulates a single layer of three clusters, based on the gene expression data. In Fig. 4(a) (Golub-1999-v1), we see that the AML samples are segregated into cluster 1, while the ALL samples are divided amongst clusters 2 and 3; that is, the PDM partition indicates that there exists structure, distinct from noise (as defined through the resampled null model), that distinguishes the ALL samples as two subtypes. If we repeat this analysis with Golub-1999-v2, we obtain the partitions shown in Fig. 4(b). Since the actual gene expression data is identical, the PDM partitioning of samples is the same; however, we now can see that the division of the ALL samples between clusters 2 and 3 corresponds to the B- and T-cell subtypes. One can readily—particularly in the context of cancers—situations in which unknown sample subclasses exist that could be detected via PDM (as in Fig. 4(a)); at the same time, the PDM’s comparison to the resampled null model prevents artificial partitions of the data.

In Figures 4(c) and (d), we see how the first layer of clustering is refined in the second layer; for example, in Fig. 4(c), the E2A-PBX1 and T-ALL leukemias are distinguished in the first layer, while the second serves to separate the MLL and majority of the TEL-AML subtypes from the mixture of B-cell ALLs in the first cluster of layer 1. As in Figs. 4(a) and (b), the PDM identifies clusters of subtypes that may not be known a priori (cf results for Yeoh-2002-v1 in Supplement, for which all the B-cell ALLs had the same class label but were partitioned, as in Fig. 4(c), by several subtypes). In Fig. 4(d), second layer cluster assignment in Fig. 4(d) distinguishes the ovarian (OV) and kidney (KI) samples from the others in the mixed cluster 2 in the first layer.

Results for the complete set of Affymetrix benchmark data are given as Supplementary Information. A  $t$ -test comparison of adjusted Rand indices obtained from the PDM suggests that it is comparable to those obtained with the best method, FMG, in [9]. However, it is important to note that this is achieved by the

PDM in an entirely unsupervised way (in contrast to the heuristic approach used to select  $k$  and  $l$  in [9]), a considerable advantage. We also note that the PDM performance remained high regardless of the distance metric used (see supplement), and we did not observe the large decrease in accuracy noted by [9] when using a Euclidean metric in spectral clustering. We attribute this largely to the aforementioned improvements (multiple layers; data-driven  $k$  and  $l$  parameterization) of PDM over standard spectral clustering.

## Pathway-PDM Analysis

The above applications of the PDM illustrate its ability to detect clusters of samples with common exposures and phenotypes based on genome-wide expression patterns, without advance knowledge of the number of sample categories. However, it is often of greater interest to identify a set of genes that govern the distinction between samples. Pathway-based application of the PDM permits this by systematically subsetting the genes in known pathways (here, based on KEGG [35] annotations), and partitioning the samples. Pathways yielding cluster assignments that correspond to sample characteristics can then be inferred to be associated with that characteristic.

We applied pathway-PDM as described above to the radiation response data from [18], testing the clustering results obtained for inhomogeneity with respect to the phenotype ( $\chi^2$  test). Because some pathways contain a fairly large number of probes, it is reasonable to ask whether the pathways that permitted clusterings corresponding to tumor status were simply sampling the overall gene expression space. In order to assess this, we also constructed artificial pathways of the same size as each real pathway by randomly selecting the appropriate number of probes, and recomputing the clustering and  $\chi^2$   $p$ -value as described above. 1000 such random pathways were created for each unique pathway length, and the fraction  $f_{\text{rand}}$  of pathways that yielded a  $\chi^2$   $p$ -value smaller than that observed in the “true” pathway is used as an additional measure of the pathway significance. Six pathways distinguished the radiation-sensitive samples with  $f_{\text{rand}} < 0.05$  as shown in Fig. 5; several also articulated exposure-associated partitions in addition to the phenotype-associated partition. Interestingly, all of the high-scoring pathways separated the high-RS case samples, but did not subdivide the three control sample classes; this finding, as well as the exposure-independent clustering assignments in several pathways in Fig. 5, suggests that there are systematic gene expression differences between the radiation-sensitive patients and all others. Several other pathways (see Supplemental Information) yield exposure-associated partitions without distinguishing between phenotypes; unsurprisingly, these are the cell cycle, p53 signaling, base excision repair, purine metabolism, MAP kinase, and apoptosis pathways.

To further illustrate Pathway-PDM, we apply it to the Singh prostate gene expression data [19] (the heavily-filtered sets from [9] have too few remaining probes to meaningfully subset by pathway). First, we observe that in the complete gene expression space, the clustering of samples corresponds to the tumor status in the second PDM layer (see Supplemental Information). This is consistent with the molecular heterogeneity of prostate cancer, and suggests that the first layer describes individual variation that is scrubbed out and then revealed in the second layer. Next, we apply pathway-PDM as described above, testing each layer of clustering for inhomogeneity with respect to the known tumor/normal labels ( $\chi^2$  test).

Of the 203 pathways considered, those that yielded significant  $f_{\text{rand}}$  in any layer of clustering is given in Table 6. No pathway yielded more than two layers of structure. A total of 29 of 203 pathways

exhibited significant clustering inhomogeneity in any layer; amongst the significant pathways, the misclassification rate—the fraction of tumor samples that are placed in a cluster that is majority non-tumor and vice-versa—is approximately 20%. Plots of the six most discriminative pathways in layers 1 and 2 are given in Figure 6.

A number of known prostate cancer related pathways appear at the top of this list. The urea acid cycle pathway, prion disease pathway, and bile acid synthesis pathways have previously been noted in relationship to prostate cancer [36]. The coagulation cascade is known to be involved in tumorigenesis through its role in angiogenesis [37], and portions of this pathway have been implicated in prostate metastasis [38]. Cytochrome P450, which is part of the inflammatory response, has been implicated in many cancers [39], including prostate [40], with the additional finding that it may play a role in estrogen metabolism (critical to certain prostate cancers) [41]. Many amino-acid metabolism pathways (a hallmark of proliferating cells) and known cancer-associated signaling pathways (Jak-STAT, Wnt) are also identified.

Because pathway-PDM does not rely upon single-gene associations and employs a “scrubbing” step to reveal progressively finer relationships, we expect that we will be able to identify pathways missed by other methods. It is of interest to compare the results obtained by pathway-PDM to those obtained by other pathway analysis techniques. In [36], the authors applied several established pathway analyses (Fisher’s test, GSEA, and the Global Test) to a suite of three prostate cancer gene expression data sets, including the Singh data considered here. Fifty-five KEGG pathways were identified in at least one data set by at least one method [36], but with poor concordance: 15 of these were found solely in the Singh data, and 13 were found in both the Singh data and at least one of the other two data sets (Welsh [42], Ernst [43]) using any method. A comparison of the pathway-PDM identified pathways to those reported in [36] is given by the final column of Table 6, which lists the data sets that yielded significance by any method (Fisher’s test, GSEA, and the Global Test) reported in [36]. Of the 29 pathway-PDM identified pathways, 16 had been identified by [36] in either the Welsh or Ernst data (including 7 found by other methods in the Singh data by [36]). The PDM-identified pathways show improved concordance with the pathways identified in [36]; while only 13 of the 40 pathways identified in the Welsh or Ernst data were corroborated by the Singh data using any method in [36], the addition of the pathway-PDM Singh results brings this to 22/40. Of the 13 pathways newly introduced in Table 6, several are already known to play a role in prostate cancer but were not detected using the methods in [36] (such as cytochrome P450, complement and coagulation cascades, and Jak-STAT signalling); several also constitute entries in KEGG that were either not present at the time that [36] was published or have had over 30% of genes added/removed, making them incomparable to the KEGG annotations used in [36]. This improved concordance supports the inferred role the PDM-identified pathways in prostate cancer, and suggests that the pathway-PDM is able to detect pathway-based gene expression patterns missed by other methods as applied to the Singh data.

## Discussion

We have presented here a new application of the Partition Decoupling Method [14, 15] to gene expression profiling data, demonstrating how it can be used to identify multi-scale relationships amongst samples using both the entire gene expression profiles and biologically-relevant gene subsets (pathways). By comparing the unsupervised groupings of samples to their phenotype, we use the PDM to infer pathways that play a

role in disease.

The PDM has a number of features that make it preferable to existing microarray analysis techniques. First, the use of spectral clustering allows identification of clusters that are not necessarily separable by linear surfaces, permitting one to identify complex relationships between samples. Importantly, this means that clusters of samples can be identified even in situations where the genes do not exhibit differential expression (ie, when they are not linearly separable); this is particularly useful when examining gene expression profiles of complex diseases, where single-gene etiologies are rare. We observe the benefit of this feature in the example of Fig. 2, where the two separate yeast cell groups could not be separated using  $k$ -means clustering but could be correctly clustered using spectral clustering, and we note that the oscillatory nature of many genes [28] makes detecting such patterns crucial.

Second, the PDM employs not only a low-dimensional embedding of the feature space, thus reducing noise (an important consideration when dealing with noisy microarray data), but also the optimal dimensionality and number of clusters is data-driven rather than heuristically set. This makes the PDM an entirely unsupervised method. Because those parameters are obtained with reference to a resampled null model, the PDM prevents samples from being clustered when the relationships amongst them are indistinguishable from noise. We observed the benefit of this feature in the radiation response data [18] shown in Fig. 3, where two (as opposed to four) phenotype-related clusters were articulated by the PDM: the first corresponding to the high-RS cases, and the second corresponding to a combination of the three control groups.

Third, the independent “layers” of clusters (decoupled partitions) obtained in PDM provide a natural means of teasing out variation due to experimental conditions, phenotypes, molecular subtypes, and non-clinically relevant heterogeneity. We observed this in the radiation response data [18], where the PDM identified the exposure groups with 100% accuracy in the first layer (Fig. 3 and Table 2) followed by highly accurate classification of the high-RS samples in the second layer (Fig. 3 and Table 5). The improved sensitivity to classify high-RS samples over linear methods (83% vs. the 64% reported using SAM in [18]) suggests that there may exist strong patterns, previously undetected, of gene expression that correlate with radiation exposure and cell type. This was also observed in the benchmark data sets [9], shown in Fig. 4 and Supplement, where the PDM automatically detected subtypes in an unsupervised manner without forcing the cluster number. The results from PDM in the radiation response data and benchmark data sets were as or more accurate than those reported using other algorithms in [18, 9], were obtained without reliance upon heuristics, and reflect statistically significant (with reference to the resampled null model) relationships between samples in the data.

The accuracy of the PDM can be used, in the context of gene subsets defined by pathways, to identify mechanisms that permit the partitioning of phenotypes. In Pathway-PDM, we subset the genes by pathway, apply the PDM, and then test whether the PDM cluster assignments reflect the known sample classes. Pathways that permit accurate partitioning by sample class contain genes with expression patterns that distinguish the classes, and may be inferred to play a role in the biological characteristics that distinguish the classes. To illustrate this, we applied Pathway-PDM to both the radiation response data [18] and a prostate cancer data set [19]. In the radiation response data [18], we identified pathways that partitioned the samples by phenotype and both by phenotype and exposure (Fig. 5) as well as pathways that only partitioned the samples by exposure without distinguishing the phenotypes (Supplement). In the prostate cancer data [19], we identified 29 pathways that partitioned the samples by tumor/normal status (Table 6).

Of these, 15 revealed the significant tumor/normal partition in the second layer rather than the first (as did the full-genome PDM, Supplement), and 13 of the 14 pathways with significant tumor/normal partitions in the first layer contained additional non-noise structure in the second; prostate cancer is known to be molecularly diverse [19], and these partitions may reflect unidentified subcategories of cancer or some other heterogeneity amongst the patients. By applying Pathway-PDM to the Singh data, we were able to improve upon the concordance reported using pathway-based analyses in [36], suggesting that the accuracy of PDM may permit the identification of significant pathways, via Pathway-PDM, that are missed by other methods.

While our application of Pathway-PDM was such that PDM clusters from each pathway were compared against known sample class labels, one can just as easily compare them to labels from the cluster assignment from full-genome PDM. Hence, for example, in a situation such as the Golub-1999-v1 data shown in Fig. 4(a), one could use the 3-cluster assignment, rather than the 2-class sample labels, to find the pathways that permit the separation of cluster-2 ALLs from the cluster-3 ALLs. In a case like this, where full-genome PDM reveals subtypes are not already known, applying Pathway-PDM may help identify the molecular mechanisms driving the subtype.

Despite these clear benefits, the PDM as applied here has a drawback: specifically, the low-dimensional nonlinear embedding of the data that makes spectral clustering and the PDM powerful also complicates the biological interpretation of the findings (in much the same way that clustering in principal component space might). Pathway-PDM serves to address this issue by leveraging expert knowledge to identify mechanisms associated with the phenotypes. Additionally, the nature of the embedding, which relies upon the geometric structure of all the samples, makes the classification of an entirely new sample challenging. These issues might be addressed in several ways: experimentally, by investigation of the Pathway-PDM identified pathways (possibly after further subsetting the genes to subsets of the pathway) to yield a better biological understanding of the dynamics of the system that were “snapshot” in the gene expression data; statistically, by modeling outcome the pathway genes using an approach such as [44] that explicitly accounts for oscillatory patterns (as seen in Fig. 2) or such as [13] that accounts for the interaction structure of the pathway; or geometrically, by implementing an out-of-sample extension for the embedding as described in [45, 46] that would allow a new sample to be classified against the PDM results of the known samples.

In sum, our findings illustrate the utility of the PDM in gene expression analysis and establish a new technique for pathway-based analysis of gene expression data that is able to articulate phenotype distinctions that arise from systems-level (rather than single-gene) differences. We expect this approach to be of use in future analysis of microarray data as a complement to existing linear techniques.

## Acknowledgments

RB would like to thank Sean Brocklebank (University of Edinburgh) for many fruitful discussions. This work was made possible by the Santa Fe Institute Complex Systems Summer School (2009). RB is supported by the Cancer Prevention Fellowship Program and a Cancer Research Training Award, National Cancer Institute, NIH.

## References

- [1] Schena M, Shalon D, Davis RW, Brown PO (1995) Quantitative monitoring of gene expression patterns with a complementary DNA microarray. *Science* 270: 467-70.
- [2] Subramanian A, Tamayo P, Mootha VK, Mukherjee S, Ebert BL, et al. (2005) Gene set enrichment analysis: a knowledge-based approach for interpreting genome-wide expression profiles. *Proc Natl Acad Sci USA* 102: 15545-50.
- [3] Eisen MB, Spellman PT, Brown PO, Botstein D (1998) Cluster analysis and display of genome-wide expression patterns. *PNAS* 95: 14863-8.
- [4] Hartigan J, Wong M (1979) Algorithm AS 136: A K-means clustering algorithm. *Applied Statistics* : 100–108.
- [5] Tavazoie S, Hughes JD, Campbell MJ, Cho RJ, Church GM (1999) Systematic determination of genetic network architecture. *Nat Genet* 22: 281-5.
- [6] Tamayo P, Slonim D, Mesirov J, Zhu Q, Kitareewan S, et al. (1999) Interpreting patterns of gene expression with self-organizing maps: methods and application to hematopoietic differentiation. *PNAS* 96: 2907-12.
- [7] D’haeseleer P (2005) How does gene expression clustering work? *Nat Biotechnol* 23: 1499-501.
- [8] Datta S, Datta S (2003) Comparisons and validation of statistical clustering techniques for microarray gene expression data. *Bioinformatics* 19: 459–466.
- [9] De Souto M, Costa I, De Araujo D, Ludermir T, Schliep A (2008) Clustering cancer gene expression data: a comparative study. *BMC bioinformatics* 9: 497.
- [10] Hastie T, Tibshirani R, Eisen MB, Alizadeh A, Levy R, et al. (2000) ‘Gene shaving’ as a method for identifying distinct sets of genes with similar expression patterns. *Genome Biol* 1: RESEARCH0003.
- [11] Li G, Ma Q, Tang H, Paterson A, Xu Y (2009) QUBIC: a qualitative biclustering algorithm for analyses of gene expression data. *Nucleic acids research* .
- [12] Hanahan D, Weinberg RA (2000) The hallmarks of cancer. *Cell* 100: 57-70.
- [13] Hudson N, Reverter A, Dalrymple B (2009) A differential wiring analysis of expression data correctly identifies the gene containing the causal mutation. *PLoS Comput Biol* 5: e1000382.
- [14] Leibon G, Pauls S, Rockmore D, Savell R (2008) Topological structures in the equities market network. *PNAS* 105: 20589–20594.
- [15] Leibon G, Pauls S, Rockmore D, Savell R (2009) Partition decomposition for roll call data. Submitted .
- [16] Kim D, Lee K, Lee D (2005) Detecting clusters of different geometrical shapes in microarray gene expression data. *Bioinformatics* 21: 1927.



- [17] Qiu P, Plevritis SK (2009) Simultaneous class discovery and classification of microarray data using spectral analysis. *J Comput Biol* 16: 935–944.
- [18] Rieger K, Hong W, Tusher V, Tang J, Tibshirani R, et al. (2004) Toxicity from radiation therapy associated with abnormal transcriptional responses to DNA damage. *PNAS* 101: 6635–6640.
- [19] Singh D, Febbo P, Ross K, Jackson D, Manola J, et al. (2002) Gene expression correlates of clinical prostate cancer behavior. *Cancer cell* 1: 203–209.
- [20] Chung F (1997) *Spectral graph theory*. Amer Mathematical Society.
- [21] Ng A, Jordan M, Weiss Y (2002) On spectral clustering: Analysis and an algorithm. *Advances in neural information processing systems* 2: 849–856.
- [22] von Luxburg U (2007) A tutorial on spectral clustering. *Statistics and Computing* 17: 395–416.
- [23] Still S, Bialek W (2004) How many clusters? An information-theoretic perspective. *Neural Computation* 16: 2483–2506.
- [24] McLachlan G, Peel D (2004) *Finite mixture models*. Wiley-Interscience.
- [25] Fraley C, Raftery A (1999) MCLUST: Software for model-based cluster analysis. *Journal of Classification* 16: 297–306.
- [26] Fraley C, Raftery A (2006) MCLUST version 3 for R: Normal mixture modeling and model-based clustering. Technical Report, Department of Statistics, University of Washington 504.
- [27] Spellman P, Sherlock G, Zhang M, Iyer V, Anders K, et al. (1998) Comprehensive identification of cell cycle-regulated genes of the yeast *saccharomyces cerevisiae* by microarray hybridization. *Molecular biology of the cell* 9: 3273.
- [28] Ptitsyn AA, Zvonic S, Gimble JM (2007) Digital signal processing reveals circadian baseline oscillation in majority of mammalian genes. *PLoS Comput Biol* 3: e120.
- [29] R Development Core Team (2004) *A language and environment for statistical computing*. Vienna, Austria.
- [30] Bolstad B, Irizarry R, Astrand M, Speed T (2003) A comparison of normalization methods for high density oligonucleotide array data based on variance and bias. *Bioinformatics* 19: 185–193.
- [31] Wheeler D, Barrett T, Benson D, Bryant S, Canese K, et al. (2007) Database resources of the National Center for Biotechnology Information. *Nucleic acids research* 35: D5.
- [32] Gentleman R, Carey V, Bates D, Bolstad B, Dettling M, et al. (2004) Bioconductor: open software development for computational biology and bioinformatics. *Genome Biol* 5: R80.
- [33] Tusher V, Tibshirani R, Chu G (2001) Significance analysis of microarrays applied to the ionizing radiation response. *Proceedings of the National Academy of Sciences of the United States of America* 98: 5116.

- [34] Golub T, Slonim D, Tamayo P, Huard C, Gaasenbeek M, et al. (1999) Molecular classification of cancer: class discovery and class prediction by gene expression monitoring. *science* 286: 531.
- [35] Kanehisa M, Araki M, Goto S, Hattori M, Hirakawa M, et al. (2008) KEGG for linking genomes to life and the environment. *Nucleic Acids Res* 36: D480-4.
- [36] Manoli T, Gretz N, Gr  
"one H, Kenzelmann M, Eils R, et al. (2006) Group testing for pathway analysis improves comparability of different microarray datasets. *Bioinformatics* 22: 2500.
- [37] Rickles F, Patierno S, Fernandez P (2003) Tissue factor, thrombin, and cancer. *Chest* 124: 58S.
- [38] Klezovitch O, Chevillet J, Mirosevich J, Roberts R, Matusik R, et al. (2004) Hepsin promotes prostate cancer progression and metastasis. *Cancer Cell* 6: 185–195.
- [39] Agúndez J (2004) Cytochrome P450 gene polymorphism and cancer. *Current Drug Metabolism* 5: 211–224.
- [40] Murata M, Watanabe M, Yamanaka M, Kubota Y, Ito H, et al. (2001) Genetic polymorphisms in cytochrome P450 (CYP) 1A1, CYP1A2, CYP2E1, glutathione S-transferase (GST) M1 and GSTT1 and susceptibility to prostate cancer in the Japanese population. *Cancer letters* 165: 171–177.
- [41] Tsuchiya Y, Nakajima M, Yokoi T (2005) Cytochrome P450-mediated metabolism of estrogens and its regulation in human. *Cancer letters* 227: 115–124.
- [42] Welsh J, Sapinoso L, Su A, Kern S, Wang-Rodriguez J, et al. (2001) Analysis of gene expression identifies candidate markers and pharmacological targets in prostate cancer. *Cancer Research* 61: 5974.
- [43] Ernst T, Hergenbahn M, Kenzelmann M, Cohen CD, Bonrouhi M, et al. (2002) Decrease and gain of gene expression are equally discriminatory markers for prostate carcinoma: a gene expression analysis on total and microdissected prostate tissue. *Am J Pathol* 160: 2169–2180.
- [44] Baker S (2010) Simple and flexible classification of gene expression microarrays via swirls and ripples. *BMC bioinformatics* 11: 452.
- [45] Bengio Y, Delalleau O, Roux N, Paiement J, Vincent P, et al. (2004) Learning eigenfunctions links spectral embedding and kernel PCA. *Neural Computation* 16: 2197–2219.
- [46] Bengio Y, Paiement J, Vincent P, Delalleau O, Le Roux N, et al. (2004) Out-of-sample extensions for LLE, IsoMap, MDS, eigenmaps, and spectral clustering. *Advances in neural information processing systems* 16: proceedings of the 2003 conference : 177.

---

**Spectral Clustering Algorithm**

---

1. Compute the correlation  $\rho_{i,j}$  between all pairs of  $n$  data points  $i$  and  $j$ .
  2. Form the affinity matrix  $\mathbf{S} \in \mathbb{R}^{n \times n}$  defined by  $s_{i,j} = \exp[-\sin^2(\arccos(\rho_{i,j}))/\sigma^2]$ , where  $\sigma$  is a scaling parameter ( $\sigma = 1$  in the reported results).
  3. Define  $\mathbf{D}$  to be the diagonal matrix whose  $(i, i)$  element is the column sums of  $\mathbf{S}$ .
  4. Define the Laplacian  $\mathbf{L} = \mathbf{I} - \mathbf{D}^{-1/2}\mathbf{S}\mathbf{D}^{-1/2}$ .
  5. Find the eigenvectors  $\{v_0, v_1, v_2, \dots, v_{n-1}\}$  with corresponding eigenvalues  $0 \leq \lambda_1 \leq \lambda_2 \leq \dots \leq \lambda_{n-1}$  of  $\mathbf{L}$ .
  6. Determine from the eigendecomposition the optimal dimensionality  $l$  and natural number of clusters  $k$  (see text).
  7. Construct the embedded data by using the first  $l$  eigenvectors to provide coordinates for the data (i.e., sample  $i$  is assigned to the point in the Laplacian eigenspace with coordinates given by the  $i$ th entries of each of the first  $l$  eigenvectors, similar to PCA).
  8. Using  $k$ -means, cluster the  $l$ -dimensional embedded data into  $k$  clusters.
- 

Table 1: Procedure for Spectral Clustering.

		Cluster		
		1	2	3
Treatment	Mock	57	0	0
	IR	0	57	0
	UV	0	0	57

Table 2: Spectral clustering of expression data versus exposure; exposure categories are reproduced exactly.

		Cluster		
		1	2	3
Treatment	Mock	36	15	6
	IR	36	15	6
	UV	3	14	40

Table 3:  $k$ -means clustering of expression data versus exposure using  $k = 3$ .

		Cluster			
		1	2	3	4
Cell type	Healthy	19	18	8	0
	Skin cancer	8	23	14	0
	Low radiation sensitivity	13	11	8	7
	High radiation sensitivity	6	1	9	26

Table 4:  $k$ -means clustering of expression data versus cell type using  $k = 4$ .

		Cluster	
		1	2
Cell type	Healthy	45	0
	Skin cancer	45	0
	Low radiation sensitivity	28	11
	High radiation sensitivity	7	35

Table 5: Spectral clustering of exposure data with exposure-correlated clusters scrubbed out, versus cell type.

KEGG Pathway	$L_p$	Layer 1		Layer 2		In [36] ?
		$p(\chi^2)$	$f_{\text{rand}}$	$p(\chi^2)$	$f_{\text{rand}}$	
00220 Urea cycle & metabolism of amino groups	33	1.14e-13	< 0.001	7.10e-01	0.940	[19, 42, 43]
00980 Metab. of xenobiotics by cytochrome P450	72	3.97e-13	0.001			—
00640 Propanoate metabolism	31	7.78e-12	0.003	9.78e-01	0.995	[42, 43]
04610 Complement and coagulation cascades	75	9.21e-12	0.008	2.47e-02	0.371	
00120 Bile acid biosynthesis	32	1.29e-01	0.699	1.15e-11	0.003	[19, 42]
05060 Prion disease	18	5.18e-02	0.527	2.20e-11	0.003	[19, 42, 43]
00380 Tryptophan metabolism	50	3.84e-11	0.008	5.52e-01	0.894	[43]
00480 Glutathione metabolism	48	4.80e-11	0.008	8.37e-01	0.955	[19, 42, 43]
04310 Wnt signaling pathway	191	5.38e-11	0.017	5.47e-01	0.916	[42]
00983 Drug metabolism - other enzymes	52	5.08e-10	0.024	8.60e-01	0.966	—
04630 Jak-STAT signaling pathway	205	1.65e-01	0.826	8.41e-10	0.025	
00053 Ascorbate and aldarate metabolism	8	3.32e-02	0.462	7.67e-09	0.008	[43]
00350 Tyrosine metabolism	45	1.32e-02	0.359	2.80e-08	0.040	[19, 42]
00641 3-Chloroacrylic acid degradation	16	5.23e-08	0.016	6.89e-01	0.893	
00960 Alkaloid biosynthesis II	8	7.13e-02	0.558	8.23e-08	0.016	[19]
00410 beta-Alanine metabolism	25	9.24e-08	0.016	1.60e-01	0.673	[43]
00650 Butanoate metabolism	37	9.39e-02	0.645	1.50e-07	0.014	
00260 Glycine, serine & threonine metabolism	36	9.56e-02	0.645	1.78e-07	0.014	[42, 43]
00600 Glycosphingolipid metabolism	32	7.84e-02	0.615	3.08e-07	0.016	[19]
00030 Pentose phosphate pathway	21	3.59e-07	0.022	2.80e-01	0.755	[42, 43]
00062 Fatty acid elongation in mitochondria	11	1.68e-01	0.684	3.67e-07	0.022	[19, 42]
00272 Cysteine metabolism	10	6.01e-07	0.025	7.52e-02	0.574	—
00340 Histidine metabolism	27	3.94e-02	0.477	1.42e-06	0.022	[43]
00720 Reductive carboxylate cycle	9	7.62e-02	0.574	1.51e-06	0.025	[19]
00565 Ether lipid metabolism	23	4.07e-06	0.036	8.43e-01	0.948	—
01032 Glycan structures - degradation	39	8.17e-01	0.957	4.62e-06	0.038	
00360 Phenylalanine metabolism	19	2.32e-02	0.376	6.26e-06	0.044	[42, 43]
00040 Pentose and glucuronate interconversions	17	7.75e-06	0.047	4.98e-01	0.843	[19]
00051 Fructose and mannose metabolism	35	4.49e-03	0.211	7.99e-06	0.043	[19, 42]

Table 6: Pathways with cluster assignment articulating tumor versus normal status in at least one PDM layer for the Singh prostate data. The  $L_p$  column lists the size of the pathway.  $\chi^2$  test  $p$ -values for tumor status versus cluster assignment in PDM layer 1 and layer 2 are given. The  $f_{\text{rand}}$  columns show the fraction of randomly-generated pathways with smaller  $\chi^2$   $p$ -values in either PDM layer. The final column lists the data sets for which [36] identified the pathway as significant ([19], Singh; [42], Welsh; [43], Ernst; a dash indicates pathways with significant revisions (>30% of genes added or removed) in KEGG between this analysis and the time of [36] publication).

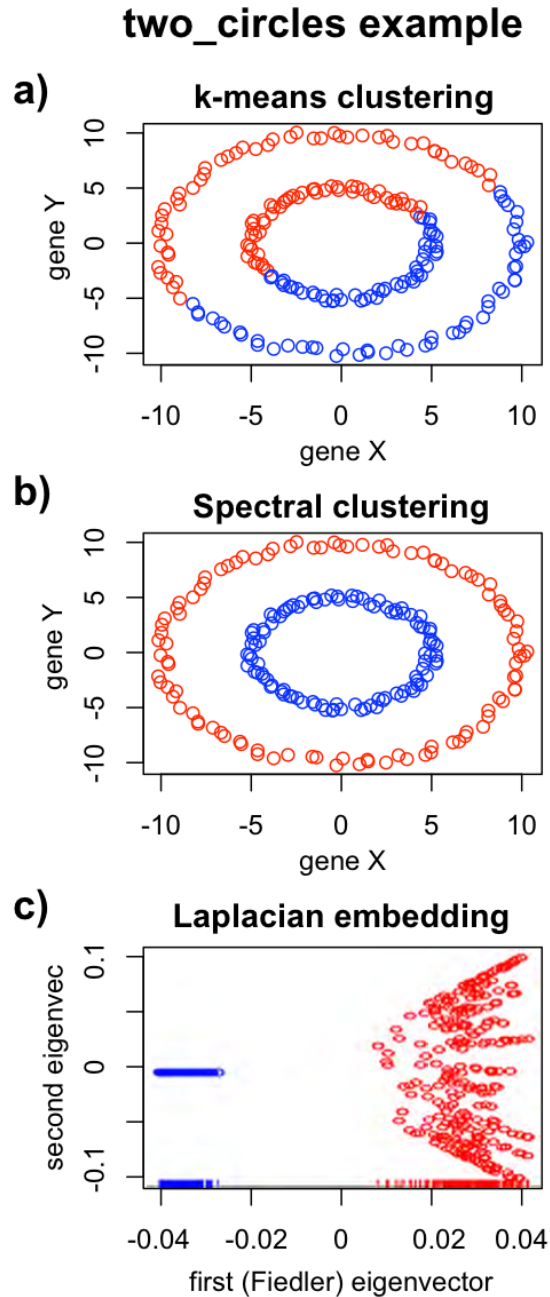


Figure 1: two\_circles examples. In (a) and (b), colors denote cluster assignments from  $k$ -means ( $k = 2$ ) and spectral clustering, respectively. In (a),  $k$ -means using  $k = 2$  produces a linear cut through the data; in the (b), spectral clustering automatically chooses two clusters and assigns clusters with nonconvex boundaries. The embedded data used in (b) is shown in (c); in this representation, the clusters are linearly separable, and a rug plot shows the bimodal density of the Fiedler vector that yielded the correct number of clusters.

## Differential amplitude in yeast cell-cycle gene expression oscillation

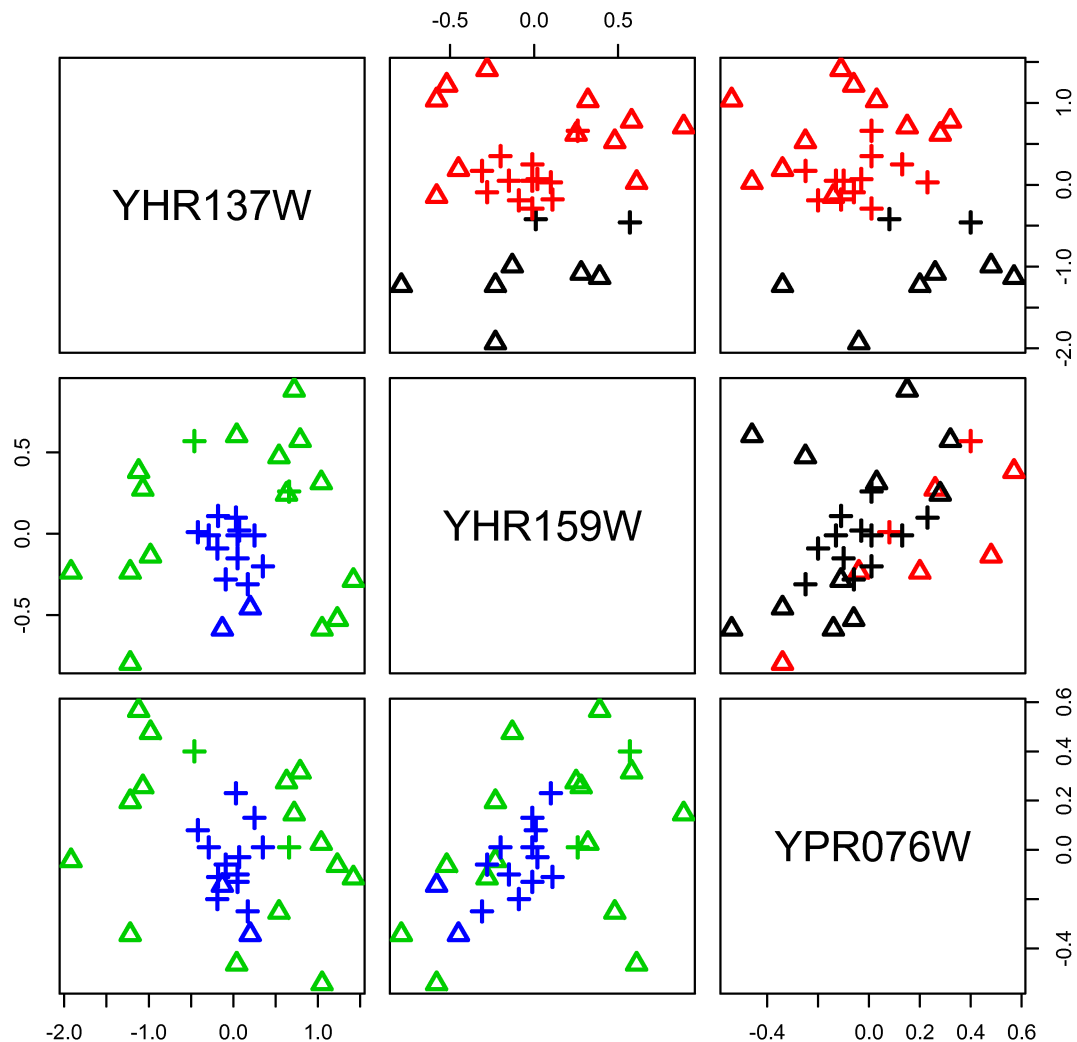


Figure 2: Yeast cell cycle data. Expression levels for three oscillatory genes are shown. The method of cell cycle synchronization is shown as shapes: crosses denote elutriation-synchronized samples, while triangles denote CDC-28 synchronized samples. Cluster assignment for each sample is shown by color; above the diagonal, points are colored by  $k$ -means clustering, with poor correspondence between cluster (color) and synchronization protocol (shapes); below the diagonal, samples are colored by spectral clustering assignment, showing clusters that correspond to the synchronization protocol.

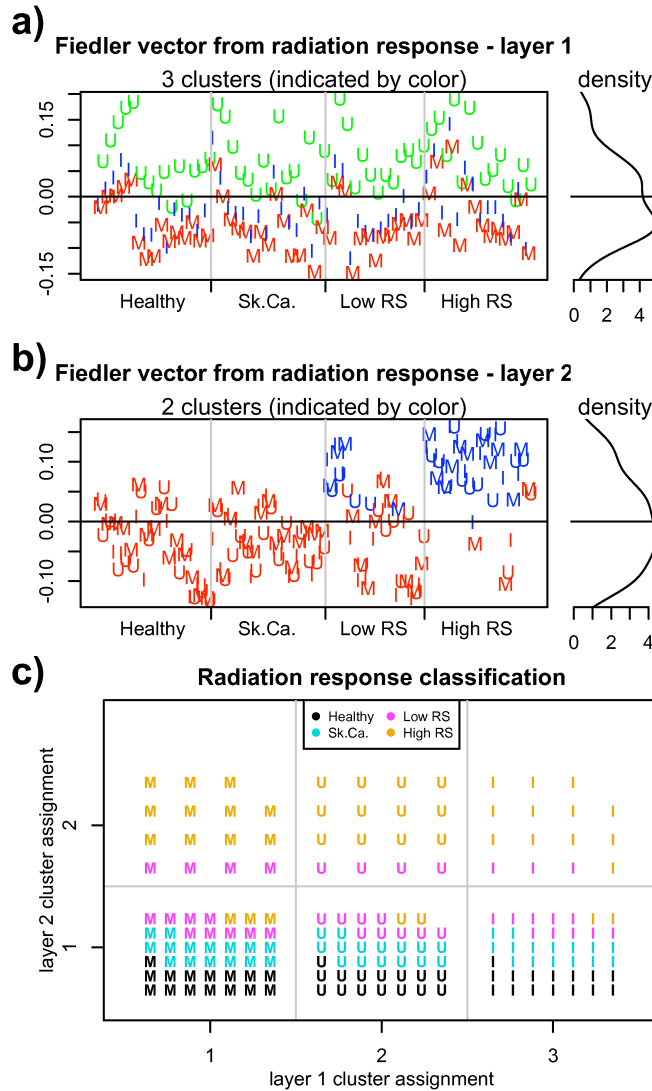


Figure 3: PDM results for radiation response data. Shown in (a) and (b) is a scatter plot of each sample's Fiedler vector value along with the resulting clustering (indicated by color) for the first (a) and second (b) PDM layers. A Gaussian mixture fit to the density (left panel) of the Fiedler vector is used to assess the number of clusters, and the resulting cluster assignment for each sample is indicated by color. Exposure is indicated by shape ("M", mock; "U", UV; "I", IR), with phenotypes (healthy, skin cancer, radiation insensitive, radiation sensitive) grouped together along the  $x$ -axis. In (a), it can be seen that the cluster assignment correlates with exposure, while in (b), cluster assignment correlates with radiation sensitivity. In (c), points are placed in the grid according to cluster assignment from layers 1 and 2 along the  $x$  and  $y$  axes; it can be seen that the UV- and IR- exposed high-sensitivity samples differ both from the mock-exposed high-sensitivity samples as well as the UV- and IR- exposed control samples.



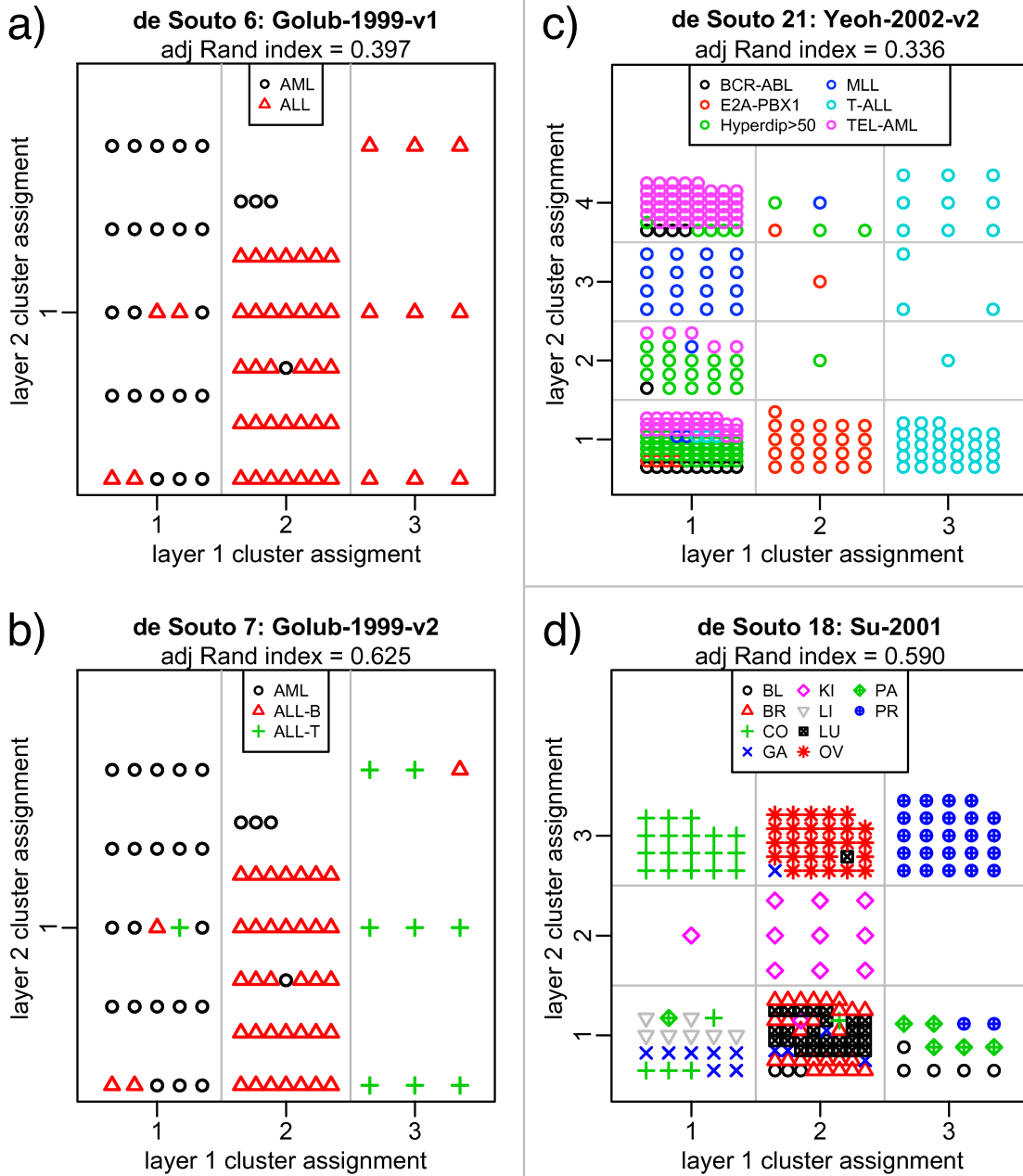


Figure 4: PDM results for several benchmark data sets. Points are placed in the grid according to cluster assignment from layers 1 and 2 (in (a) and (b) no second layer is present). In (a) and (b) it can be seen that the PDM identifies three clusters, and that the division of the ALL samples in (a) corresponds to a subtype difference (ALL-B, ALL-T) in (b). In (c) and (d), it can be seen that the partitioning of samples in the first layer is refined in the second PDM layer.

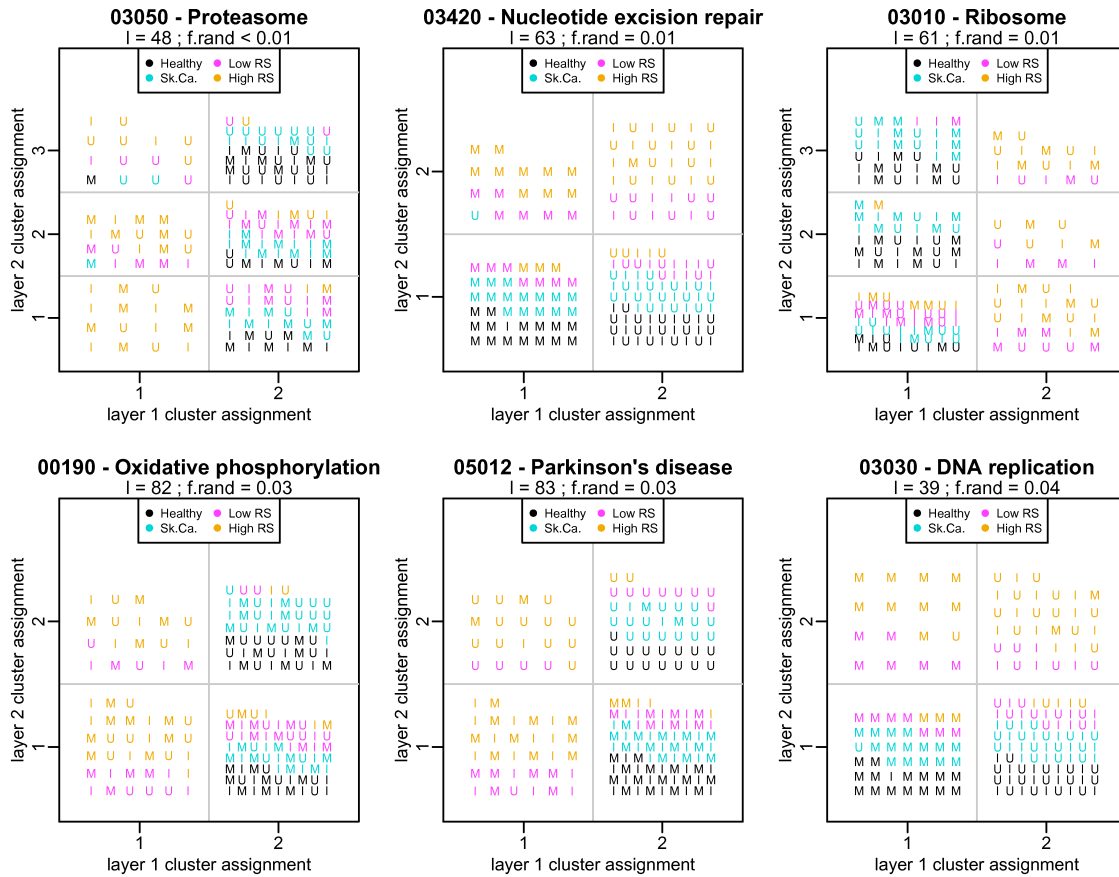


Figure 5: Pathway-PDM results for top pathways in radiation response data. Points are placed in the grid according to cluster assignment from layers 1 and 2 along for pathways with  $f_{\text{rand}} < 0.05$ . Exposure is indicated by shape (“M”, mock; “U”, UV; “I”, IR), with phenotypes (healthy, skin cancer, low RS, high RS) indicated by color. Several pathways (nucleotide excision repair, Parkinson’s disease, and DNA replication) cluster samples by exposure in one layer and phenotype in the other, suggesting that these mechanisms differ between the case and control groups.

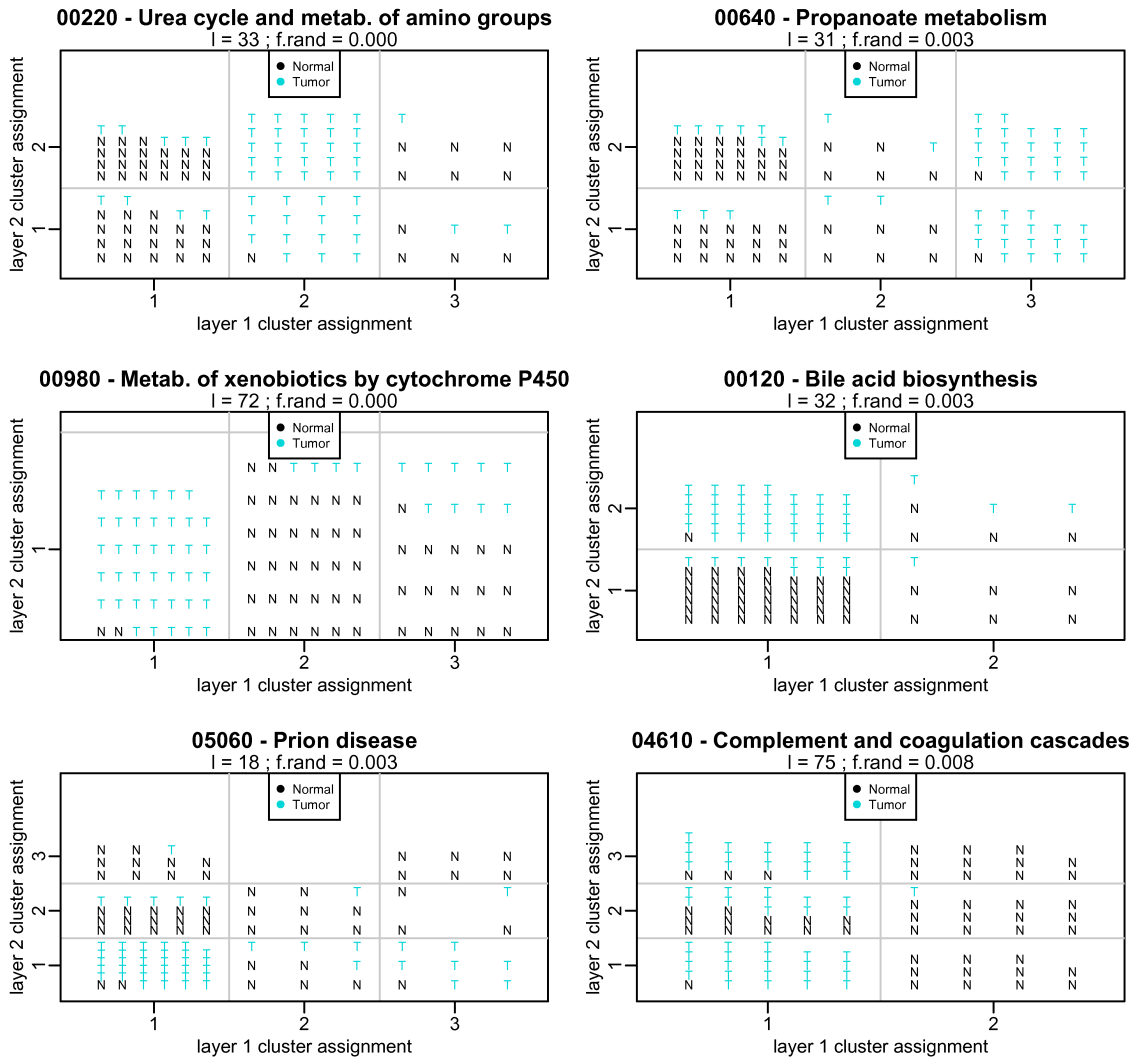


Figure 6: Pathway-PDM results for top pathways in the Singh prostate data. Points are placed in the grid according to cluster assignment from layers 1 and 2; shown are the six most discriminative pathways.

## Supplemental figures

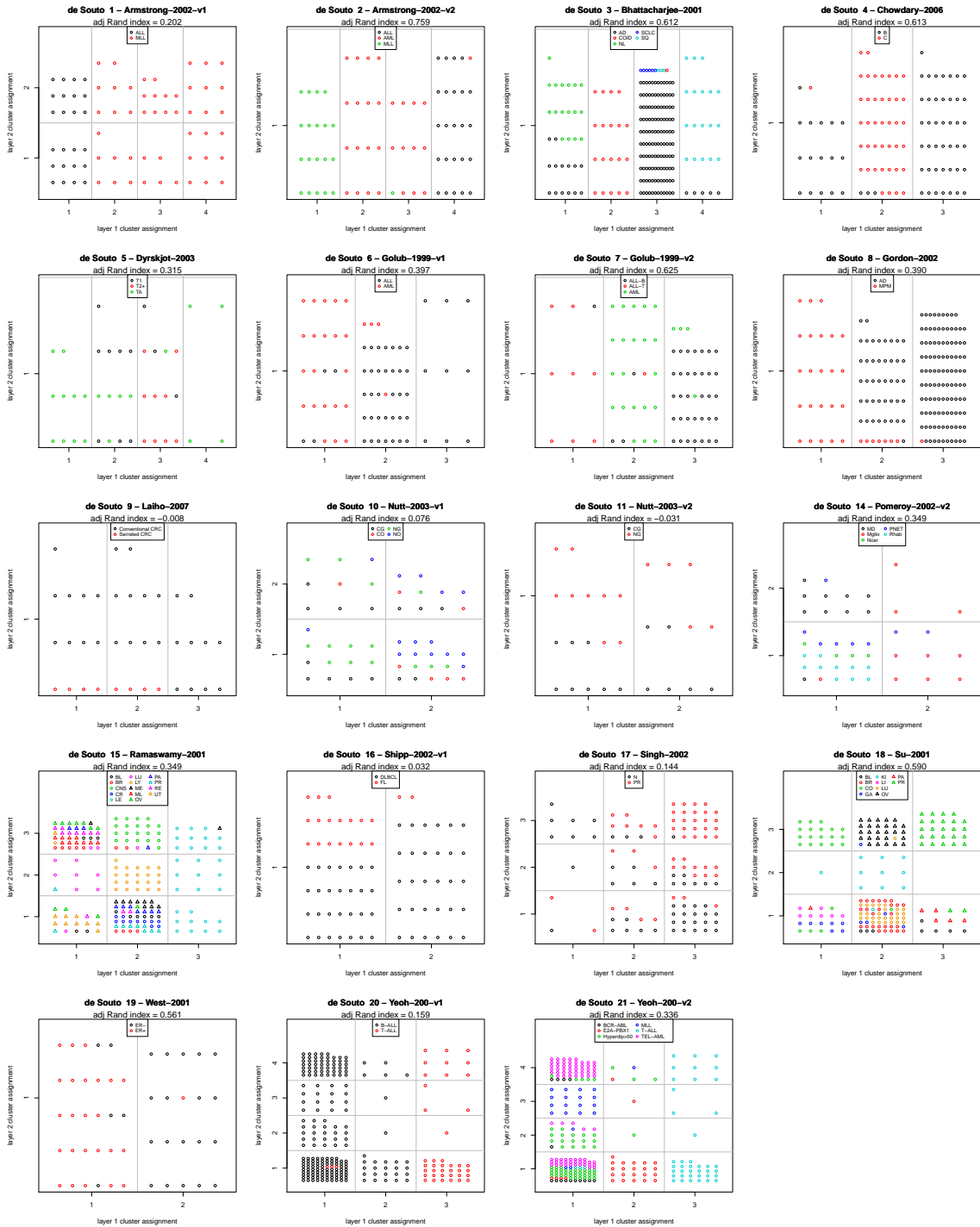


Figure S-1: PDM classifications of deSouto benchmark set samples using a correlation-based distance metric (as described in methods).

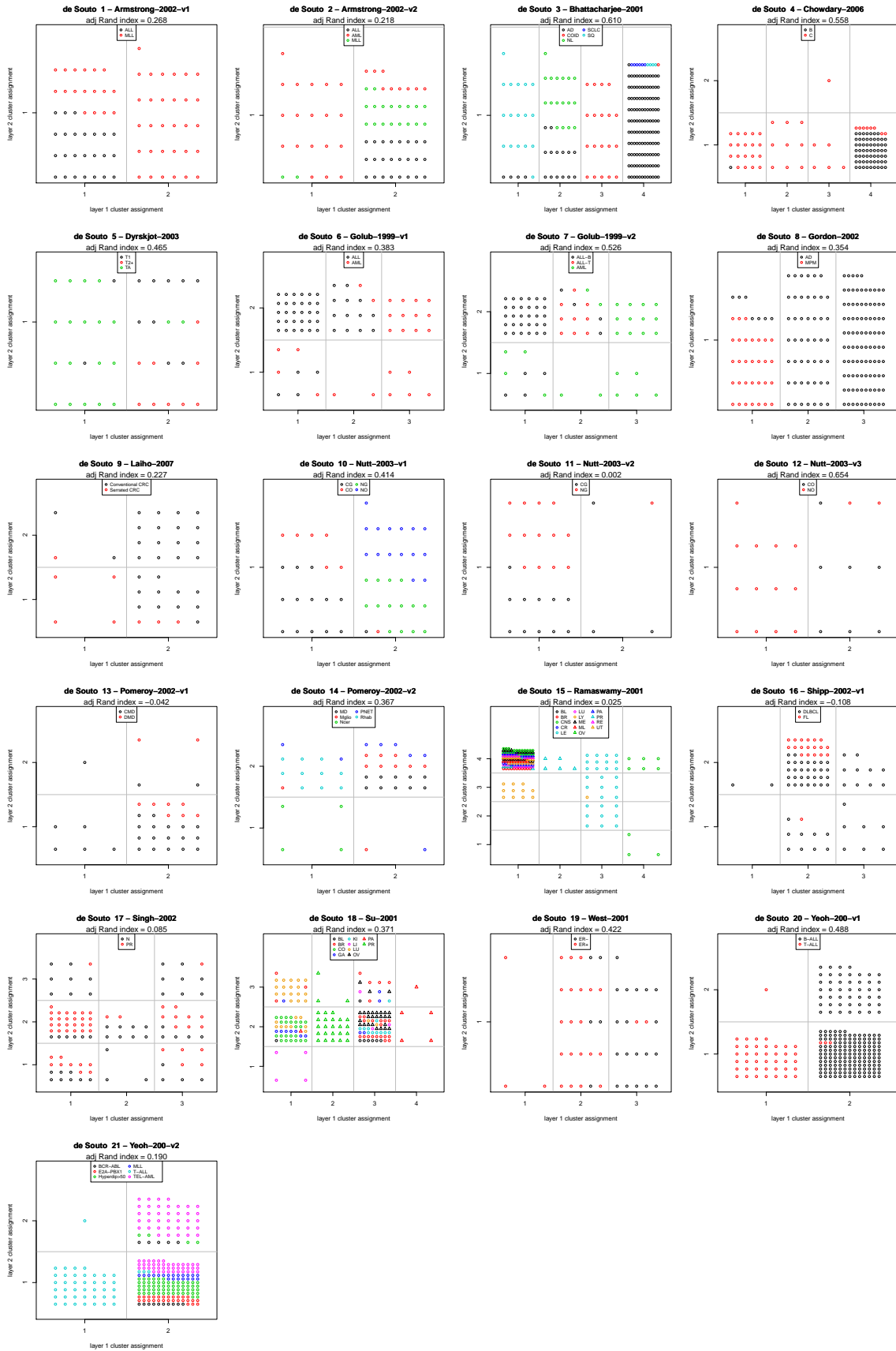


Figure S-2: PDM classifications of deSouto benchmark set samples using a Euclidean distance metric.

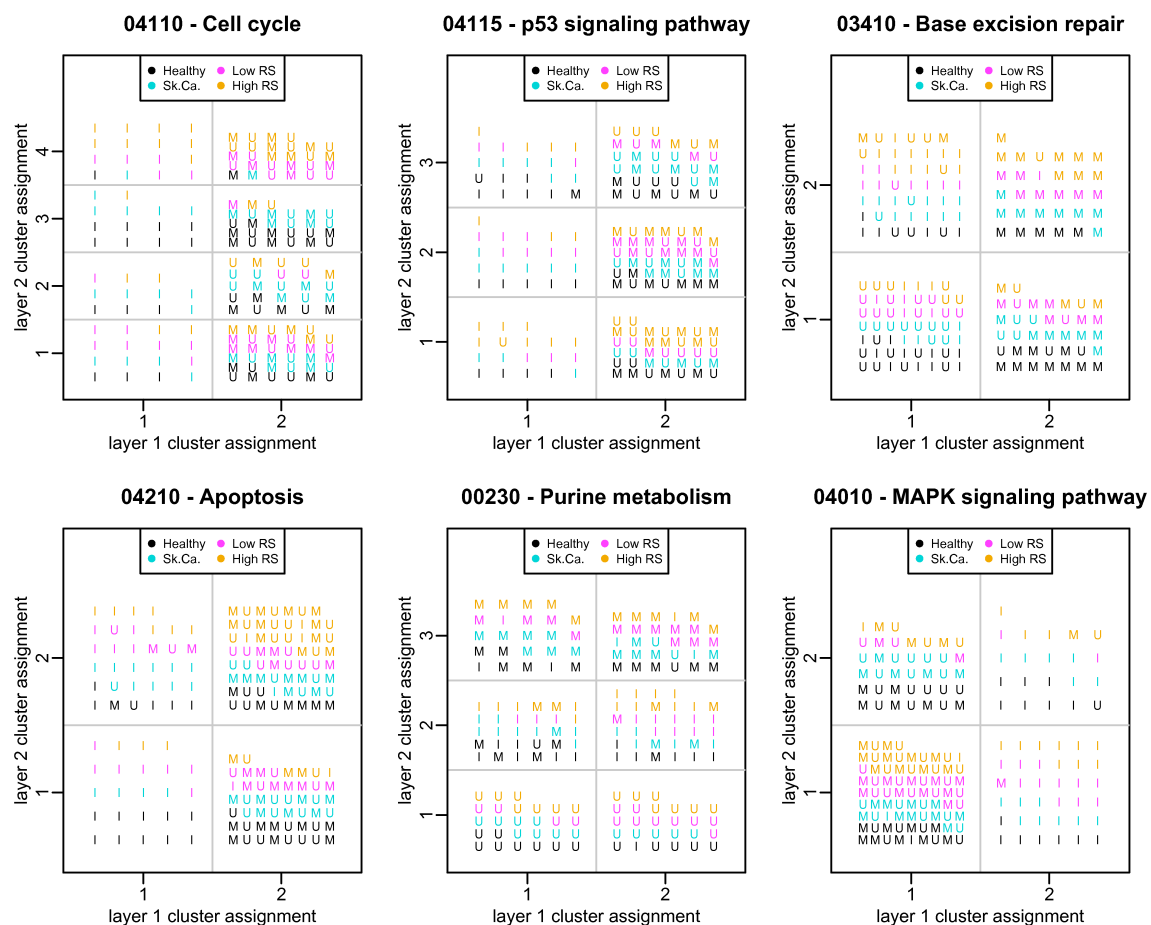


Figure S-3: Pathway-PDM classifications of radiation response data for pathways that discriminate cells by radiation exposure but not by phenotype, suggesting that these mechanisms are intact across sample types. Exposure is indicated by shape (“M”, mock; “U”, UV; “T”, IR), with phenotypes (healthy, skin cancer, low RS, high RS) indicated by color. The discriminatory pathways relate to DNA metabolism and cell death, as would be expected from radiation exposure.

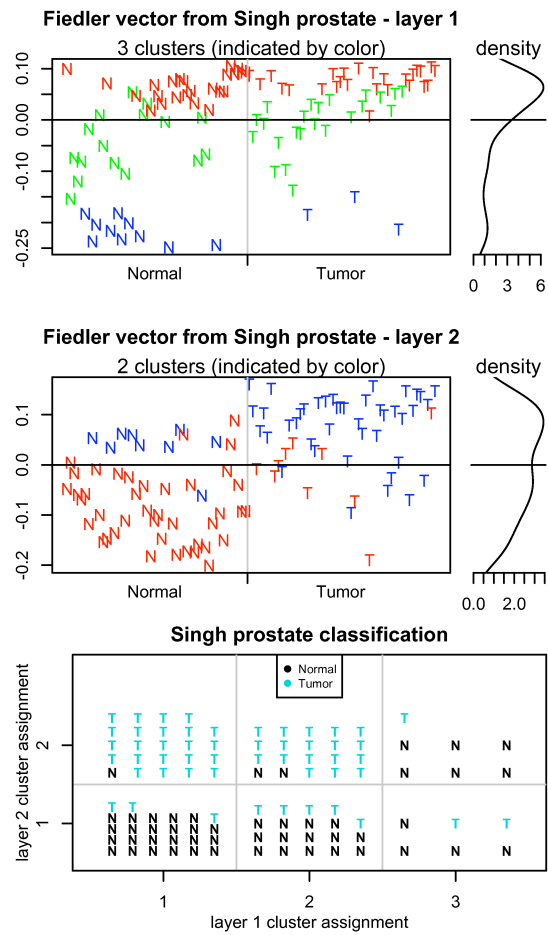


Figure S-4: PDM results in first and second layers of the Singh prostate tumor data using all genes. The top two panels show the Fiedler vector values and clustering results, along with the Fiedler vector density, in the first and second layer; the bottom panel shows the combined classification results. The second layer, but not the first, discriminates the tumor samples.